Journal of Electric Propulsion

RESEARCH

Open Access

Determining the 2D spatial distribution of plasma parameters in a cylindrical cross section of a radio-frequency ion thruster by optical emission spectroscopy

Felix Becker[1*], Pascal Sarnoch[1], Kristof Holste[1], Hans Leiter[1] and Peter J. Klar[1]

*Correspondence:
felix.becker@exp1.physik.uni-giessen.de

[1] Institute of Experimental Physics I, Justus Liebig University, Heinrich-Buff-Ring 16, 35392 Giessen, Hesse, Germany

Abstract

Gridded ion engines, such as the radio-frequency ion thruster, are highly efficient designs for generating thrust on satellites or spacecrafts for both commercial and scientific missions, due to the very high exhaust velocities achieved. A thorough understanding of the low-temperature and low-pressure plasma parameters is essential in order to characterize, design, and optimize such a thruster. Corresponding plasma parameters can be obtained non-invasively from empirical correlations between the results of Langmuir double probe measurements and optical emission spectroscopy. The plasma parameters can be extracted solely from the recorded optical emission spectra once such an empirical correlation is established for a specific experimental setup and various operation conditions. Light from an object plane at a specified depth within the plasma is focussed onto the projection plane, using a telescopic arrangement of lenses and an aperture. Despite being out of focus, the grid structure is still identifiable though slightly blurred. By carefully scanning across this image, taking spectra at every light spot, we can record a series of optical emission spectra where each spectrum corresponds to a plasma volume located in the object plane behind a grid hole. The object plane is a 2D cross section within the bulk of the plasma at a distance of 5 cm behind the grid. Our approach therefore allows us to monitor the spatial profiles of plasma parameters in this cross section of the RIT 10 for different operating points of the thruster. Such spatial profiles are essential for characterizing thruster performance and improving global modeling of such thrusters. We believe that this method is also applicable for RITs of other sizes in the context of space qualification.

Keywords: Optical emission spectroscopy (OES), Principal component analysis (PCA), Langmuir diagnostics, Electric propulsion, Radio-frequency ion thruster (RIT)

Introduction

Gridded ion thrusters (GITs) are a prominent class of electric propulsion (EP) systems for space applications. These thrusters utilize a high-voltage grid system to create electrostatic fields that accelerate ions to high velocities, resulting in high specific impulse and high mass efficiency [1]. In comparison, other EP devices, such as, for example, electron cyclotron resonance (ECR) thrusters with a magnetic nozzle or Hall thrusters [2], may yield higher levels of thrust but require significantly more propellant per thrust unit [3]. For missions prioritizing mass efficiency, radio-frequency ion thrusters (RITs), a subset of GITs, enable longer mission durations or greater payload capacities [1, 4, 5]. More satellite and scientific missions intend to use GITs as their main thruster due to these and other benefits. Therefore, the need for rapid, reliable and non invasive methods to characterize the thruster plasma has increased [4, 6, 7]. Having detailed information about the plasma is key to understanding and optimizing the operation of such an engine and to predicting its performance [8]. However, measurement approaches that directly probe the plasma are typically required to obtain key properties such as electron temperature and ion density. The plasma in RITs is very confined and inaccessible for measurements using invasive probes such as Langmuir probes. Also, the effects of the alternating electromagnetic field generating the plasma increases complexity in the measurement process in the case of RITs specifically [9].

Obtaining spatial information about the plasma is challenging. One approach is to manually move a Langmuir probe within the plasma. This approach is highly invasive and poses a significant experimental challenge [10–13]. Another approach that yields information about the plasma parameters is the analysis of the beam profile. It is easier to conduct than measurements with invasive probes inside the plasma, but is a rather indirect measurement [14, 15]. In this work, we present an approach where we measure the spatial distribution of electron temperature and ion density of the plasma by evaluating optical emission (OE) spectra using a preestablished bijective empirical correlation between OE spectra and Langmuir probe measurements. The underlying idea was discussed and proven previously [16–18]. Once this correlation between the non-invasively obtained OE data and the invasively measured Langmuir probe data is established, this measurement approach enables rapid and non-invasive determination of plasma parameters. Since this approach relies on light emitted by the plasma, we use a telescopic arrangement of lenses and an aperture to carefully select the volume inside the plasma from which the light is originating for our spectroscopic analysis. The work presented here demonstrates this capability. This measurement scheme provides the possibility of measuring spatial variations of the plasma inside a RIT non-invasively.

Correlation between plasma parameters and OE spectra

Experimental setup and measurement procedures

A scheme of the experimental setup utilized in this study is illustrated in Fig. 1. The experiment is composed of two important parts. On the left hand side, the RIT with the electronics needed to operate the thruster and the Langmuir probe diagnostics mounted through the gas inlet of the thruster and its source measure unit (SMU) are depicted. On the right hand side the telescopic lens arrangement and the spectroscopic setup are depicted. The thruster employed is a RIT-10 type model thruster featuring a cylindrical discharge chamber with a diameter of 10cm and an extraction system comprising three grids. Xenon plasma is generated using a radio-frequency generator (RFG) [19, 20] operating at a frequency of approximately 1.5MHz. No voltages are applied to the grids. The thruster operates in grounded mode without a neutralizer.

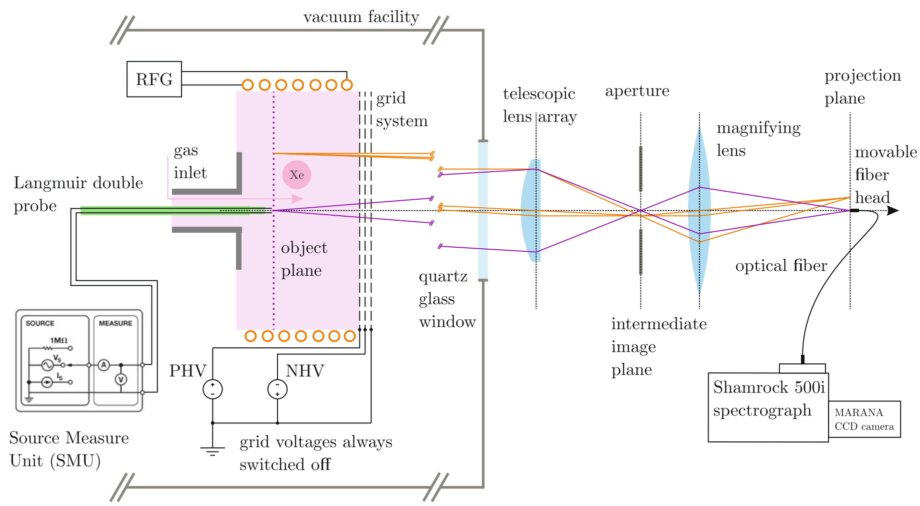

Fig. 1 Schematic representation of the experimental setup for establishing a correlation between Langmuir probe data and optical emission spectra as well as for spatial mapping. The Langmuir probe consists of a ceramic tube and two tungsten wires located in the object plane. The image of the tip of the Langmuir probe in the projection plane is focused onto the input slit of the Shamrock 500i spectrograph. Spectra taken from the central position analyze light mainly originating from the volume around the tip of the probe. This is achieved by employing a telescopic arrangement of a camera objective, an aperture in the intermediate image plane and another lens for focussing light from the image plane onto the fiber facet attached to the spectrometer. In a correlation measurement, both Langmuir probe measurements and OE measurements are taken simultaneously for different operating points of the thruster, covering a wide range of operation, i.e., combinations of power settings supplied to the radio frequency generator and values of xenon mass flow. No voltages are applied to the grids. In the mapping measurement, the movable fiber head is moved to different positions in the projection plane. The blurred out of focus image of the extraction grid system serves as a reference frame of the spatial positions

Optical emission (OE) spectroscopy measurements are conducted from outside the vacuum chamber through a window transparent to wavelengths ranging from 200nm to 1μm. Light from the plasma in the object plane is focused onto the facet of an optical fiber located in the projection plane via a telescopic lens arrangement, which is then connected to a Shamrock 500i Spectrograph using a Marana CCD Camera as detector. Each spectrum contains 401 data points, each representing a wavelength and intensity value within the range of 824 to 876 nm. Each spectrum is accumulated with a total acquisition time of 50 s.

The Langmuir double probe is inserted into the thruster through the gas inlet to measure plasma parameters. Our design of the Langmuir double probe follows the recommendations outlined in the work of Lobbia [21]. The Langmuir double probe consists of two tungsten wires each with a diameter of 0.3 mm, arranged parallel to each other and extending 4.5 mm into the plasma. The main ceramic tube, which houses both wires, is divided towards the end where the two wire ends forming the tip are located. This results in individual ceramic tubes, one for each wire. The wires protrude approximately 4 mm out of the ceramic tubes and are separated by a gap of 1.5 mm. This design addresses the issue of metal deposits on the insulating material, which can occur when operating the probe at high voltages due to sputtering of the tip material. Such metal deposits on top of the ceramic insulator can lead to short-circuit currents between the wire ends. In this design, the thick insulator between the two metal wire ends enhances the quality of the inserted probe. In our setup, the instrument operates with voltages sweeping between −60 V to 60 V for up to 200 hours without notable deterioration in measurement quality. The analysis of the Langmuir data for extracting the plasma parameters, i.e., electron temperature and electron density will be described in the next section.

The OES of the plasma inside the discharge chamber of the thruster is conducted as follows. We use a telescope setup to image the entire object plane where the tips of the Langmuir probe are located into a projection plane outside the vacuum chamber. The object plane is parallel to the grid plane, but spatially separated by a distance of 5 cm along the thruster axis into the plasma. Nevertheless, the arrangement of the grid holes is still visible in the projection plane, though blurred as it is not in focus which defines a spatial reference frame for the spatial mapping of the plasma.

The simultaneous recording of the OE spectra and the Langmuir data at the same location inside the plasma (correlation measurement), which is necessary to establish a bijective correlation between the plasma parameters and the intensities of the optical emission lines, is conducted as follows. The tip of the Langmuir double probe inserted into the center of the discharge chamber of the mounted thruster via the gas inlet is illuminated by a laser for alignment. The laser light scattered by the probe tip is imaged onto the intermediate image plane by the camera objective ($f_1 = 13$ cm). This procedure defines the location of the object plane (highlighted in Fig. 1) where the plasma parameters will be mapped as described below (mapping measurement). The intermediate image plane is already located outside the vacuum chamber. An aperture with an opening diameter of about 1.5 cm is positioned in the intermediate image plane. This aperture surrounds the demagnified intermediate image of the objective plane and somewhat suppresses light not coming from the objective plane. The intermediate image is imaged and magnified onto the projection plane using a second lens ($f_2 = 9$ cm). The entry facet of the optical fiber connected to the OE spectrometer is positioned in this plane. It can be moved to different locations in the projection plane in order to collect light originating from the corresponding positions in the object plane. The image of the tip of the Langmuir double probe is in the center of the projection plane and on the line of sight of the telescope arrangement. The line of sight points to the probe tip and passes the central hole of the grid system.

For the *correlation measurement*, the entry facet of the fiber is positioned on the sharp image of the probe tip, which is overlaid by the blurred image of the central grid hole. This ensures that in the correlation measurement mainly light from a small volume around the tip of the Langmuir probe is detected. After completing the alignment, the thruster is operated in a wide range of operating parameters with no applied grid voltages. For this purpose, the mass low is varied from 2 to 5.5 sccm and the RFG power varied from 40 to 120 W. This results in 72 distinct operating points. At each of these individual operating points defined by a pair of RFG power and mass flow values, a measurement of a Langmuir voltage-current characteristic and an OE spectrum are recorded after about 1 hour of thruster operation needed for the thruster system to reach a state of thermal equilibrium with the vacuum chamber. The procedure to correlate the data of the two measurements is described in "Principal component analysis of the OE spectra" section.

The *mapping measurement* yields a spatial mapping of the plasma parameters in the object plane. It can be carried out for a given specific operating point of the thruster based on the bijective correlation established between OE spectral intensities and plasma parameters. The blurred image of the grid holes superimposed on the sharp image of the objective plane in the projective plane serves as a reference coordinate frame of the in-plane coordinates of the object plane. One OE spectrum is recorded at each reference point defined by the blurred image of a corresponding grid hole. This is done by moving the fiber facet to the corresponding position in the projection plane. The recording of the OE spectra at the reference point for the specific operating point is carried out after thruster and vacuum chamber have reached thermal equilibrium. For a reliable mapping, it is of paramount importance that thruster operation is stable and that none of the components of the optical system is altered, but the position of the fiber facet. How the spatial distribution of the plasma parameters for the given operating point is derived on the basis of the spatial map of OE spectra and the bijective correlation is described in detail in "Spatial distribution of the plasma parameters in a cylindrical cross section of the RIT-10 discharge vessel" section.

Analysis of the Langmuir double probe measurements

The voltage-current characteristic obtained by a voltage sweep from −60 V to 60 V of the voltage applied between the wire ends of the Langmuir double probe inserted into the plasma is analyzed to extract the electron temperature T_e and electron density n_e [21, 22]. It holds that electron density n_e equals to the propellant ion density n_i in case of the RIT 10 at the operating points studied because the singly charged ion species, i.e., Xe^+, dominates. The evaluation procedure is described in more detail in our previous publications [16–18] and involves normalizing all current values by the saturation current. Subsequently, the electron temperature is derived from the largest slope s of the third-order polynomial fit in the vicinity of the origin using

$$T_e = \frac{e}{2k_B \cdot s}. \tag{1}$$

Finally, the saturation regions of the Langmuir double probe characteristic are fitted with linear fits in the outer regions of the curve. The saturation current I_sat is then calculated using the intercept of the polynomial function fitted to the saturation current and the linear function through the turning point. This yields the ion density [17] using:

$$n_i = \frac{I_\mathrm{sat}}{e \cdot A_\mathrm{probe}} \cdot \sqrt{\frac{M_\mathrm{xenon}}{k_B \cdot T_e}}. \tag{2}$$

The voltages of n_i and T_e determined for the different operational points are shown in Fig. 2. Both plasma parameters show the expected trends. For a given mass flow, ion density and electron temperature increase with increasing power coupled into the plasma. For a given power, the ion density increases with increasing mass flow, whereas the electron temperature decreases. It is worth noting that the data pairs of plasma parameters for all operating points studied are different.

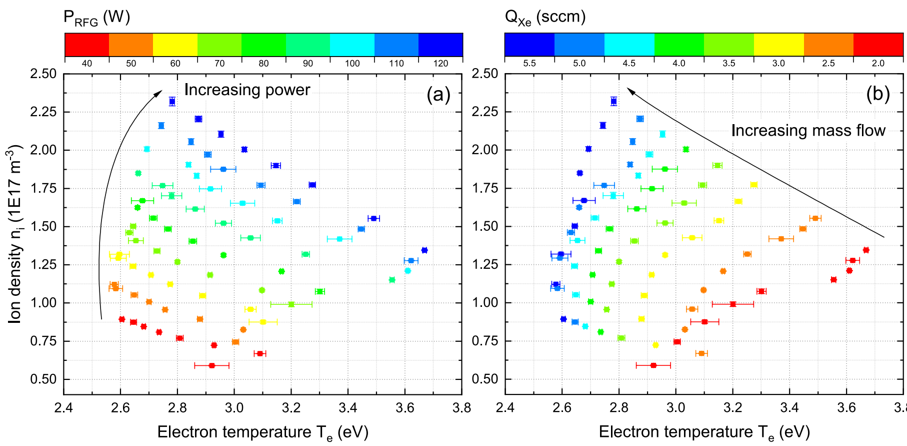

Fig. 2 Plots of the Langmuir probe data. Ion density vs electron temperature for 72 operating points of the RIT 10. In (**a**) the data is colored with respect to the power supplied to the RFG and in (**b**) with respect to the mass flow. All data is derived from the voltage-current characteristics of a Langmuir double probe measured at the corresponding operating point of the thruster. The probe is located in the center of the plasma

Principal component analysis of the OE spectra

The optical spectra obtained from the OE measurements contain 401 data pairs of intensity value and wavelength position each. This means that a spectrum can be interpreted as a single point in a coordinate space with as many dimensions. In particular, in the case of atomic line spectra, the spectral information is compressed in a small number of wavelength intervals corresponding to intensity peaks (lines) of dipole-allowed electronic transitions. Therefore, it usually turns out to be sufficient to establish a bijective correlation between the intensity characteristics of these lines in the OE spectra and the plasma parameters extracted from the Langmuir probe data. In our case, we restrict ourselves to the analysis of the three optical transitions emitted at center wavelengths of 828.01, 834.68 and 840.92 nm in air, i.e., this approach essentially allows us to reduce the 401-dimensional coordinate space to 3 dimensions. All three lines correspond to transitions of the neutral xenon atom [23, 24]

$$
\begin{aligned}
\lambda_{828.01} &: 5p^5\left({}^2\mathrm{P}_{3/2}\right)6p\,[1/2]_0 \rightarrow 5p^5\left({}^2\mathrm{P}_{3/2}\right)6s\,[3/2]_1'\\
\lambda_{834.68} &: 5p^5\left({}^2\mathrm{P}_{1/2}\right)6p\,[3/2]_2 \rightarrow 5p^5\left({}^2\mathrm{P}_{1/2}\right)6s\,[1/2]_1'\\
\lambda_{840.92} &: 5p^5\left({}^2\mathrm{P}_{3/2}\right)6p\,[3/2]_1 \rightarrow 5p^5\left({}^2\mathrm{P}_{3/2}\right)6s\,[3/2]_2'.
\end{aligned}
\tag{3}
$$

The spectrum of the plasma emission also reveals lines corresponding to optical transitions of singly ionized xenon, but these are much weaker and not considered in our analysis. For further evaluation, each spectrum is background corrected and area-normalized to its total intensity. The normalization contributes to the stability of the data analysis, in the sense that, in this case, only relative intensity changes between the three emission lines play a role in establishing the correlation between the OE spectra and the plasma parameters for the different operating points. Furthermore, it makes the analysis less prone to intensity changes originating, for example, from unintended movement of equipment or staining of the optical window during testing. On the other hand, it sacrifices somewhat obvious properties of the spectra, e.g., increased overall intensity with increasing excitation power or increasing propellant mass flow.

For each area-normalized OE spectrum, the intensity peaks of the three chosen optical transitions are fitted to a Voigt function in order to determine the peak areas as a measure of their relative intensity. All the analyzed peaks exhibit a full-width at half-maximum of approximately 0.6 nm given by the spectral resolution of the spectrometer used. Each OE spectrum is now reduced to three intensity values, i.e., described by a coordinate vector with three components. This procedure produces the dataset used in the principal component analysis (PCA). Therefore, the spectrum measured for a specific set of operating parameters of the thruster is represented by a single point in the three-dimensional coordinate system where the axes correspond to the relative intensity values of the three transitions. We denote the vector of coordinates corresponding to a spectrum as $\overrightarrow{S}$.

A PCA essentially conducts a rotation of this 3-dimensional coordinate system such that the new 3-dimensional coordinate system is based on the eigenvectors of the covariance matrix of the set of coordinate vectors $\left\{\overrightarrow{S}\right\}$. The covariance matrix is a 3×3 matrix. Its eigenvectors, the new coordinates, are the so called principal components (PC_i) [25] and they are ordered with descending weight of the total variance, i.e., PC_1 has the highest variance, PC_2 the second highest variance etc. The spectrum which was previously represented by the three-dimensional vector $\overrightarrow{S}$ containing the relative intensities of the three chosen optical transitions can be written as a linear combination of the three PC_i, thus, is now represented by the corresponding set of scores a_i given by

$$\overrightarrow{S} = \overrightarrow{\langle S \rangle} + \underbrace{a_1\overrightarrow{PC_1}}_{\approx 85\%\ \text{variance}} + \underbrace{a_2\overrightarrow{PC_2}}_{\approx 13\%\ \text{variance}} + \underbrace{a_3\overrightarrow{PC_3}}_{\approx 2\%\ \text{variance}} \tag{4}$$

It turns out that the representation of the spectra by pairs of scores (a_i, a_j) of any of the three combinations of PCs does not allow a full separation of the spectra in a 2D plane. However, such a full separation can be achieved by using two new coordinates X_rot and Y_rot given as linear combinations of the three eigenvectors *PC*<spanclass='convertEndash'>1−3 according to

$$\begin{aligned} X_\mathrm{rot} &= 0.35 \cdot \mathrm{PC1} - 0.94 \cdot \mathrm{PC2} + 0 \cdot \mathrm{PC3} \\ Y_\mathrm{rot} &= -0.45 \cdot \mathrm{PC1} - 0.17 \cdot \mathrm{PC2} - 0.88 \cdot \mathrm{PC3} \end{aligned} \tag{5}$$

to span the 2D plane. The multiplicative factors given in Eq. 2.3 are rounded to the second decimal place.

The landscapes of the electron temperature and ion (electron) density of the 72 different operating points as a function of the new coordinates X_rot and Y_rot are given in Fig. 3. In both cases, an equidistant 20×20 mesh is generated covering the 2D dataset of the 72 data points (X_rot, Y_rot) of the 72 distinct operating points. Based on this mesh a Renka-Cline interpolation for electron temperature and ion density is conducted. The interpolated plasma parameters $T_e(X_\mathrm{rot}, Y_\mathrm{rot})$ and $n_i(X_\mathrm{rot}, Y_\mathrm{rot})$ on the equidistant 2D mesh are then each fitted to a 5th degree 2D polynomial function in order to parameterize the surfaces of the two landscapes. The results are depicted in Fig. 4a, b.

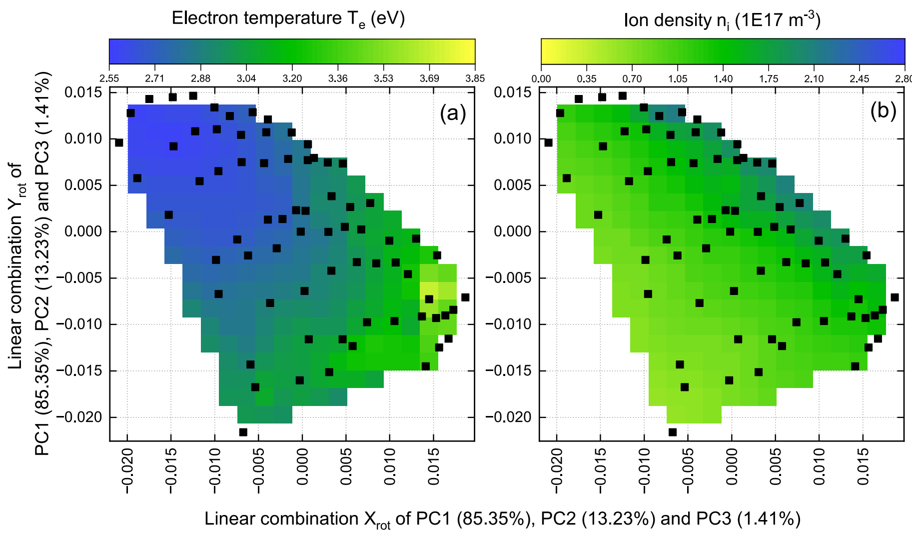

Fig. 3 Electron temperature and ion density versus PCA based coordinates. Colour plots of electron temperature and ion density for the 72 operating points of the thruster plotted in a 2D coordinate system (X_{rot} , Y_{rot}) where X_{rot} and Y_{rot} are linear combinations of the principal components which separate all operational points

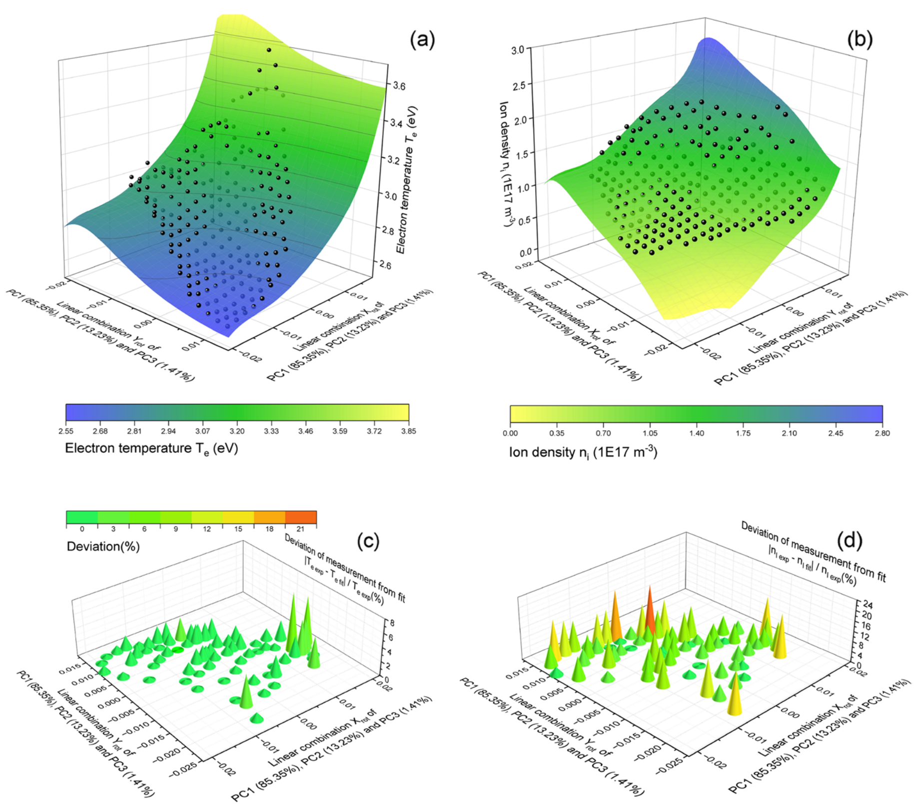

Fig. 4 Correlation functions linking OE spectra to T_e and n_e. Parametrization of the (**a**) electron temperature and (**b**) ion density correlating OE spectra and plasma parameters. **c**, **d** Relative errors between parametrization of the plasma parameters and the actual measured values for all 72 operating points of the thruster of the correlation measurement

The deviation between the original data for both, the electron temperature and ion density, and the corresponding values calculated using the fitted function are plotted in Fig. 4c, d. The absolute values of the average deviation (largest deviation) from the experimental data are 0.3 eV (8.3%) and $0.47 \cdot 10^{17} \frac{1}{m^{-3}}$ (21.1%) for electron temperature and ion density, respectively. The largest deviations for the ion density is notably higher in the edge regions of the fitted area. Nevertheless, the data remains well-represented, particularly given the uncertainties inherent in measuring plasma parameters with Langmuir probes. Furthermore, the analysis of the spatial dependence of the plasma parameters primarily requires a good agreement on the central region of the parameter space (see also the discussion of Fig. 5b below).

The parameterizations $T_e\,(X_{\mathrm{rot}}, Y_{\mathrm{rot}})$ and $n_i\,(X_{\mathrm{rot}}, Y_{\mathrm{rot}})$ are the outcome of the correlation measurement representing the bijective correlation between the OE spectra and the plasma parameters. These two parameterizations of the plasma parameters will be the basis for the analysis of their spatial distribution in a cross section of the cylindrical vessel parallel to the grid system of at a depth of about 5 cm for a specific operation point of the RIT (mapping measurement) described in the next section.

Spatial distribution of the plasma parameters in a cylindrical cross section of the RIT-10 discharge vessel

Extraction of spatial distributions of plasma parameters from OE mappings

We conducted mapping measurements for three different operating points of the thruster. The RFG excitation power at all three operating points was 80 W corresponding to an intermediate power in terms of the power variation used in the correlation measurement. The three operating points differed in terms of mass flow used, i.e., 3, 4, and 5 sccm. However, all three mass flow values are again in the intermediate range of the mass flow variation used in the correlation measurement. As described in "Experimental setup and measurement procedures" section, the weak and blurred (out of focus) image of the grid system superimposed on the focussed projection image of the object plane serves as spatial reference coordinate frame where the

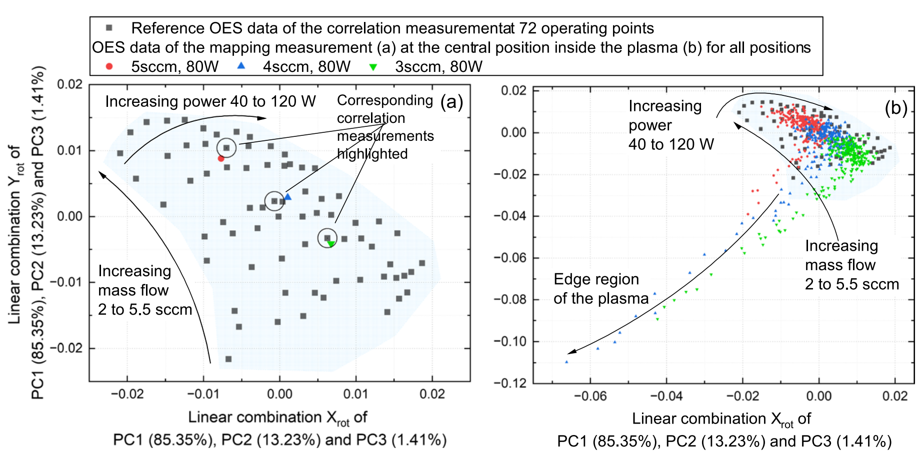

Fig. 5 Comparison of OES derived coordinates $\left(X'_{\mathrm{rot}}, Y'_{\mathrm{rot}}\right)$ of the mapping measurement with the coordinates $(X_{\mathrm{rot}}, Y_{\mathrm{rot}})$ of the correlation measurement. Only the coordinate pairs of the mapping measurement that overlap with the reference data set of the correlation measurement are considered for further analysis

sites of the 241 grid holes define the spatial locations in the object plane. A mapping measurement for a specific operating point comprises 241 OE spectra. Thus, for the three operating points, 743 OE spectra have to be analyzed following the procedure described above ("Principal component analysis of the OE spectra" section). Each spectrum of three mappings is background corrected and area normalized, prior to extracting the relative line intensities at center wavelengths of 828.01, 834.68l, and 840.92 nm by fitting and to yielding a corresponding 3-dimensional vector of coordinates $\overrightarrow{S}'$. The scores of each $\overrightarrow{S}'$ with respect to the PCs of the reference data set derived by the correlation measurements is calculated as follows

$$\overrightarrow{PC}_i \cdot \left(\overrightarrow{S}' - \overrightarrow{\langle S \rangle}\right) = a_i', \tag{6}$$

The scores can be used to calculate the coordinate pair $\left(X'_{\mathrm{rot}}, Y'_{\mathrm{rot}}\right)$ and derive from those the local plasma parameters using the parameterization functions of the plasma parameter landscapes as $T_e\left(X'_{\mathrm{rot}}, Y'_{\mathrm{rot}}\right)$ and $n_i\left(X'_{\mathrm{rot}}, Y'_{\mathrm{rot}}\right)$.

First, we will discuss the reliability and reproducibility of the score or coordinate pair determination when moving the fiber facet between reference positions in the projection plane. Corresponding results are shown in Fig. 5. Figure 5a shows the coordinate pairs $(X_{\mathrm{rot}}, Y_{\mathrm{rot}})$ based on the scores of the correlation OES measurements conducted for the 72 different operating points of the thruster. The scores used are based on the PCA of the OE spectra taken at the central position of the reference frame which corresponds to the center hole position in the superimposed blurred image of the grid system. The shaded blue area indicates the 2D range of coordinate pairs $(X_{\mathrm{rot}}, Y_{\mathrm{rot}})$ where the parameterization of the plasma parameters based on the reference measurements holds. The coloured symbols in the graph, on the other hand, correspond to coordinate pairs $\left(X'_{\mathrm{rot}}, Y'_{\mathrm{rot}}\right)$ derived for the OE spectra taken at the center of the reference frame in the three mapping measurements (80 W RFG power and 3, 4, and 5 sccm mass, respectively). The calculation of these coordinate pairs is based on Eq. (6). The circles in the graph surround the symbols of the coordinate pairs $(X_{\mathrm{rot}}, Y_{\mathrm{rot}})$ taken at the same position of the reference frame for the same operational points, the black ones correspond to the correlation measurement and the coloured ones to the mapping measurements. It should be noted that the correlation measurement and the mapping measurements have been performed on different days. Furthermore, the operating point as well as the position of the fiber facet has been altered between measurements. The very good agreement between the coordinate pairs derived from OE spectra taken in the different measurements reflects the stability of the experimental set up and the repeatability of the data acquisition process, which is essential for the validity of our measurement approach.

Figure 5b shows the coordinates $\left(X'_{\mathrm{rot}}, Y'_{\mathrm{rot}}\right)$ of all the OE spectra recorded across the grid in the three mapping measurements for the three different operating points. The coordinates $\left(X'_{\mathrm{rot}}, Y'_{\mathrm{rot}}\right)$ are again determined by Eq. (6). Almost all coordinates lie in the shaded blue area indicating the 2D range of coordinate pairs $(X_{\mathrm{rot}}, Y_{\mathrm{rot}})$ of the correlation measurement. A few coordinate pairs $\left(X'_{\mathrm{rot}}, Y'_{\mathrm{rot}}\right)$ belonging to OE spectra of the mappings taken at the edges of the grid lie outside the shaded area. Those data points are not shown and discarded in the spatial analysis of the plasma parameters as they lie outside the range where the parameterization of the plasma parameters deduced from the correlation measurement is valid. Furthermore, the coordinates $\left(X'_{\mathrm{rot}}, Y'_{\mathrm{rot}}\right)$ of each mapping form a cloud of data points and the three clouds indicated by the three colours are shifted with respect to each other.

Spatial mappings of the plasma parameters

The results of the 2D spatial analysis of the plasma parameters are depicted in Fig. 6 for the three selected operating points. The electron temperatures (graphs (a) to (c)) vary between about 2.6 eV and 3.5 eV over all three operating points. The average electron temperature decreases with increasing mass flow. At each operating point, the lowest electron temperature of the cross section is located in the center of the plasma with the electron temperature increasing towards the wall of the discharge chamber. This finding is expected as the energy coupling into the plasma occurs via the RF-coil surrounding the discharge chamber. Thus, the energy coupling is the more efficient the closer the local plasma volume is to the coil windings. This general trend is to be expected for RITs, but has not been measured this detailed before. The precise values and local variations as shown in Fig. 6a to c, when compared with simulations, will provide valuable insight in the thermal properties of the plasma and will be useful for further optimization of the thruster. Furthermore, we also observe clear and consistent trends for the spatial ion density profiles in Fig. 6d to f. The ion density varies over the three operating points between $0.6 \cdot 10^{17}$ and $2 \cdot 10^{17} \mathrm{m}^{-3}$. At the two operating points with lower propellant mass flow (Fig. 6e to f) the ion density essentially increases in the radial direction

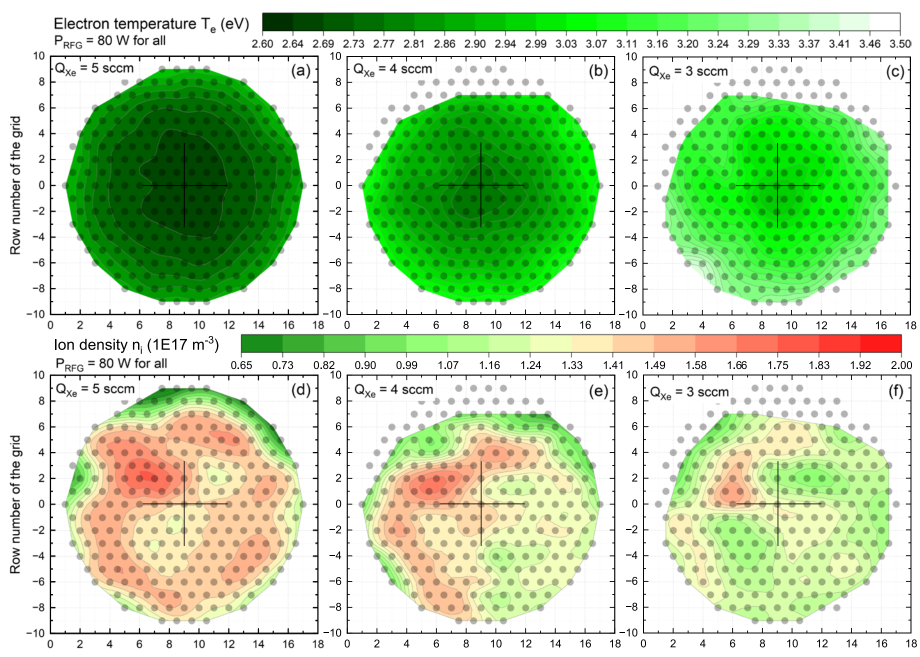

Fig. 6 2D spatially resolved maps of the plasma parameters in a cylindrical cross section of the RIT 10. **a**-**c** Electron temperature T_e and (**d**-**f**) ion density n_i for a radio-frequency power of 80 W and xenon mass flows of 5, 4, and 3 sccm. Each map shows as an overlay the front view of the 241 grid holes of the RIT 10 type model thruster, with grid hole positions marked as light gray circles. The overlay serves as a spatial reference frame of the cross section

towards the center of the cross section. However, at the highest mass flow (Fig. 6d), the behaviour of the spatial ion density in the 2D cross section is somewhat different. It seems that a ring of high ion density is surrounding the center which exhibits a lower ion density. A very similar observation has previously been made in 3D particle-in-cell simulations of RITs [26–28] and in spatially resolved Langmuir probe measurements via the grid of a RIT-like ion source [10].

In addition, we observe a density hotspot in the plasma in the spatial ion density profiles which is consistently visible in at all three operating points. It is centered in the second row and sixth column of the reference grid. At this location, the ion density is locally increased by approximately 25 %. We believe that the local maximum in ion density may be caused by the fraction of the RF-coil wound around the discharge chamber closest to the 2D cross-section of the plasma in the object plane imaged by the telescopic lens arrangement used in the mapping measurement. Identifying such hotspots or other anomalies within the ion density of the plasma is possible in our measurements because of the high spatial resolution achievable in the OES mapping measurement. Such findings will be very helpful in characterizing thrusters and identifying possible failure mechanisms. Understanding the origin of such localized variations in the spatially resolved plasma parameters, will contribute to optimizing thruster performance and life time.

A subset of data is plotted for both electron temperature and ion density as a function of spatial position in Fig. 7a, b. The data are those along the central row of the reference frame. These plots give an alternative presentation of the quantitative changes of the plasma parameters between the three operating points. Furthermore, the graphs of Fig. 7c-d show waterfall-like plots of the corresponding background-corrected and area-normalized OE spectra acquired along the central row of the reference frame. The series of spectra exhibit only subtle differences as a function of positions across the reference frame which are challenging to assess by the naked eye, but, as demonstrated, can be reliably picked up by the PCA based approach presented in this work.

Conclusion and outlook

In summary, we propose a PCA-based approach of using OE spectroscopy for a non-invasive determination of the spatial distribution of plasma parameters inside an operating RIT 10. It turns out to be a powerful for plasma characterization provided that a reliable reference data set is available and a bijective empirical correlation between OE spectra and plasma parameters extracted from Langmuir probe measurements has been established. The ability to precisely measure spatial distributions of plasma parameters enables further optimization of ion thruster performance and design. In particular, the discovery of local hotspots and density anomalies within the plasma provides valuable insights critical for understanding and improving thruster lifetime and efficiency. Such spatial distributions of plasma parameters are otherwise difficult to obtain experimentally, in particular, in the case of gridded ion thrusters where the plasma fully surrounded by thruster components, i.e., discharge vessel and extraction grid system. In general, our PCA-based approach founded on optical emission spectroscopy is very useful in measuring properties of plasma parameters

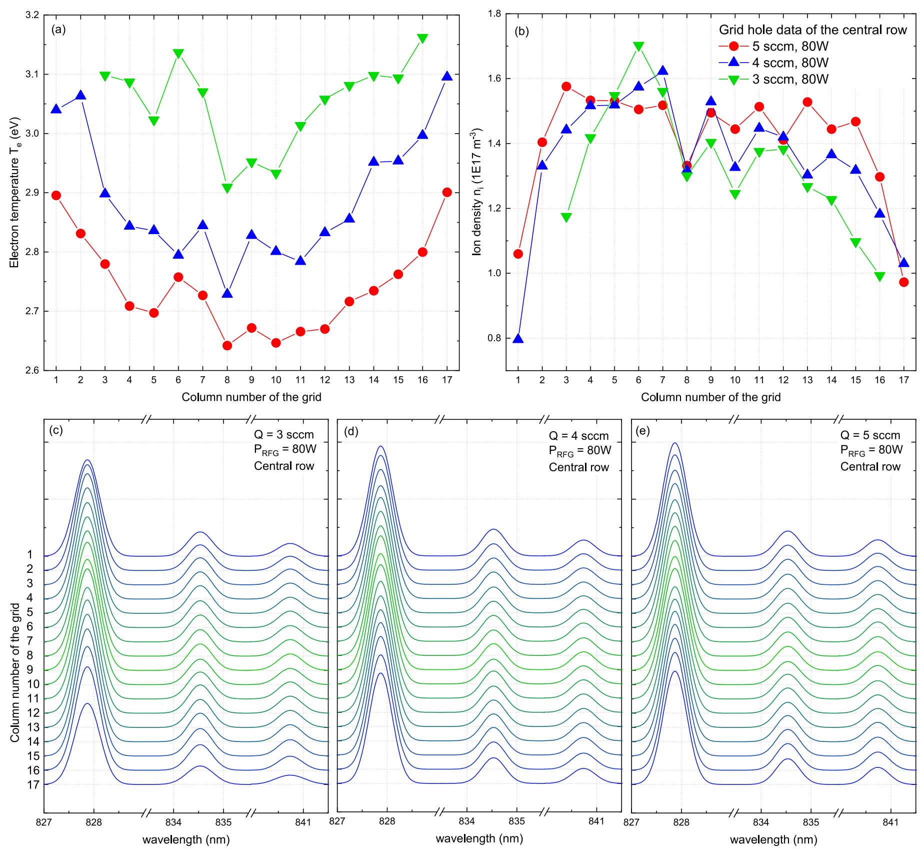

Fig. 7 Line plots of the spatially resolved plasma parameters in the central horizontal row of the reference frame given by the grid holes. **a** electron temperature T_e (**b**) the ion density n_i, P_{RFG} is 80 W for all measurements and the mass flow of xenon is varied between 5, 4 and 3 sccm. The graphs present the variation of plasma parameters across the central, horizontal row of the reference frame given by the grid holes. **c**, **d** Waterfall-plots of the background-corrected and area-normalized OE spectra along the central horizontal row of the reference frame derived by mapping measurements at the three operating points

which are otherwise difficult to assess. For example, in addition to spatially resolved measurements of plasma parameters of RITs, it should also be possible to monitor the temporal behaviour of the plasma parameters during periodic cycles of the plasma excitation by performing time-resolved optical emission spectroscopic measurements [17]. Therefore, we believe that our approach after further refinement will provide a new plasma diagnostic tool which may even be used for characterizing flight models of thrusters. It will enable a monitoring of the plasma parameters in RITs as well as other thruster types with a high spatial and temporal resolution and reveal further correlations between plasma parameters and thruster designs which are essential for validating plasma simulation models of thrusters and enhancing their predictive power.

Acknowledgements
F.B. thanks Ariane Group for funding of his PhD studentship in the frame of the JLU-AGG graduate school "radiofrequency ion thrusters".

Authors' contributions
F.B. wrote the main manuscript text. F.B. and P.S. conducted the experiments. F.B. prepared all figures. All authors reviewed the manuscript and provided feedback.

Funding
Open Access funding enabled and organized by Projekt DEAL.

Data availability
Data that support the findings of this study have been deposited in the JLU's internal repository, JLUpub, and are available under the following link: https://jlupub.ub.uni-giessen.de/handle/jlupub/20147.

Declarations

Competing interests
The authors declare no competing interests.

Received: 13 January 2025 Accepted: 15 February 2025
Published online: 27 February 2025

References

1. Holste K, Dietz P, Scharmann S, Keil K, Henning T, Zschätzsch D, Reitemeyer M, Nauschütt B, Kiefer F, Kunze F, Zorn J, Heiliger C, Joshi N, Probst U, Thüringer R, Volkmar C, Packan D, Peterschmitt S, Brinkmann KT, Zaunick HG, Thoma MH, Kretschmer M, Leiter HJ, Schippers S, Hannemann K, Klar PJ (2020) Ion thrusters for electric propulsion: Scientific issues developing a niche technology into a game changer. Rev Sci Instrum 91(6):061101. https://doi.org/10.1063/5.0010134
2. Mazouffre S (2016) Electric propulsion for satellites and spacecraft: established technologies and novel approaches. Plasma Sources Sci Technol 25(3):033002. https://doi.org/10.1088/0963-0252/25/3/033002
3. Goebel DM, Katz I, Mikellides IG (2023) Fundamentals of electric propulsion. John Wiley & Sons
4. Leiter HJ, Kukies R, Porst JP, Kuhmann J, Berger M, Rath M (2014) Results from the rit-22 technology maturity demonstration activity. In: 50th AIAA/ASME/SAE/ASEE Joint Propulsion Conference. Aerospace Research Central: Cleveland, p 3421
5. Feili D, Loeb H, Schartner K, Weis S, Kirmse D, Meyer B, Kilinger R, Mueller H, Di Cara DM (2005) Performance mapping of new án-rits at giessen. In: IPEC, vol 252. Electric Rocket Propulsion Society: Princeton
6. Killinger R, Kukies R, van Holtz L, Tomasetto A (2002) Orbit raising with ion propulsion on esa's artemis satellite. In: 38th AIAA/ASME/SAE/ASEE Joint Propulsion Conference & Exhibit. Aerospace Research Central: Indianapolis, p 3672
7. Leiter HJ, Loeb HW, Schartner KH (2000) The RIT 15 Ion Engines-A Survey of the Present State of Radio Frequency Ion Thruster Technology and its Future Potentiality. In: Spacecraft Propulsion, vol 465. Harvard University: Cannes, p 423
8. Leiter HJ (2000) Entwicklung und physikalische Untersuchung eines Hochfrequenz-Ionentriebwerks unter besonderer Berücksichtigung des Extraktionsgittersystems und der Ionisatorform. Ph.D. Thesis. Justus-Liebig-Universität Gießen, Germany
9. Oksuz L, Soberón F, Ellingboe AR (2006) Analysis of uncompensated langmuir probe characteristics in radio-frequency discharges revisited. J Appl Phys 99(1). https://doi.org/10.1063/1.2158496
10. Schäfer M (1971) Plasmadiagnostik und Energiebilanzuntersuchung an dem HF-Ionentriebwerk RIT 10. Ph.D. Thesis. Naturwissenschaftliche Fakultät, Justus-Liebig-Universität Gießen, Germany
11. Masherov P, Riaby V, Abgaryan V (2016) Evaluation of ion current density distribution on an extraction electrode of a radio frequency ion thruster. Plasma Sources Sci Technol 26(1):015004. https://doi.org/10.1088/0963-0252/26/1/015004
12. Schwabedissen A, Benck EC, Roberts JR (1997) Langmuir probe measurements in an inductively coupled plasma source. Phys Rev E 55(3):3450–3459. https://doi.org/10.1103/physreve.55.3450
13. Hopwood J, Guarnieri CR, Whitehair SJ, Cuomo JJ (1993) Langmuir probe measurements of a radio frequency induction plasma. J Vac Sci Technol A Vac Surf Films 11(1):152–156. https://doi.org/10.1116/1.578282
14. Mühlich NS, Holste K, Klar PJ, Leiter HJ (2017) Near-field beam diagnostics for radio-frequency ion thrusters rit. In: Proceedings of the 35th International Electric Propulsion Conference, Atlanta
15. Reeh A, Probst U, Klar PJ (2019) Global model of a radio-frequency ion thruster based on a holistic treatment of electron and ion density profiles. Eur Phys J D 73(11). https://doi.org/10.1140/epjd/e2019-100002-3
16. Becker F, Nauschütt B, Chen L, Holste K, Klar PJ (2023) Plasma parameter measurement on a RIT-10 using empirical correlations between non-invasive optical emission spectroscopy and langmuir diagnostics. J Electr Propuls 2(1). https://doi.org/10.1007/s44205-023-00052-z
17. Nauschütt BT, Chen L, Holste K, Klar PJ (2021) Non-invasive assessment of plasma parameters inside an ion thruster combining optical emission spectroscopy and principal component analysis. EPJ Tech Instrum 8(1). https://doi.org/10.1140/epjti/s40485-021-00070-x
18. Nauschütt B, Chen L, Holste K, Klar PJ (2022) Combination of optical emission spectroscopy and multivariate data analysis techniques as a versatile non-invasive tool for characterizing xenon/krypton mixed gas plasma inside operating ion thrusters. J Appl Phys 131(5). https://doi.org/10.1063/5.0074412
19. Simon J, Probst U, Klar PJ (2016) Development of a radio-frequency generator for rf ion thrusters. Trans Jpn Soc Aeronaut Space Sci Aerosp Technol Jpn 14(ists30):33–39
20. Junker J, Probst U, Klar P (2019) Development of a full bridge series resonant radio-frequency generator for optimized rit operation. In: 36th International Electric Propulsion Conference, Vienna
21. Lobbia RB, Beal BE (2017) Recommended practice for use of langmuir probes in electric propulsion testing. J Propuls Power 33(3):566–581. https://doi.org/10.2514/1.b35531
22. Chen FF (2003) Langmuir probe diagnostics. In: IEEE-ICOPS Meeting, vol 2. Citeseer, Jeju

23. Kramida A, Ralchenko Y (1999) Nist atomic spectra database, nist standard reference database 78. https://doi.org/10.18434/T4W30F
24. Priti Gangwar RK, Srivastava R (2019) Collisional-radiative model of xenon plasma with calculated electron-impact fine-structure excitation cross-sections. Plasma Sources Sci Technol 28(2):025003. https://doi.org/10.1088/1361-6595/aaf95f
25. Abdi H, Williams LJ (2010) Principal component analysis. WIREs. Comput Stat 2(4):433–459. https://doi.org/10.1002/wics.101
26. Henrich R (2013) Development of a plasma simulation tool for radio frequency ion thrusters. Ph.D. Thesis. Justus-Liebig-University Giessen, Germany
27. Turkoz E, Celik M (2014) 2-D electromagnetic and fluid models for inductively coupled plasma for RF ion thruster performance evaluation. IEEE Trans Plasma Sci 42(1):235–240. https://doi.org/10.1109/tps.2013.2287903
28. Volkmar C, Neumann A, Geile C, Hannemann K (2017) Real-time in situ determination of inductively coupled power and numerical prediction of power distribution in RF ion thrusters. In: Proceedings of the 35th International Electric Propulsion Conference, Atlanta